NeuroImage: Clinical 27 (2020) 102293

Contents lists available at ScienceDirect

NeuroImage: Clinical

journal homepage: www.elsevier.com/locate/ynicl

Axonal damage in the optic radiation assessed by white matter tract integrity metrics is associated with retinal thinning in multiple sclerosis

Chanon Ngamsombat[a,b], Qiyuan Tian[a], Qiuyun Fan[a], Andrew Russo[c], Natalya Machado[c], Maya Polackal[a], Ilena C. George[c], Thomas Witzel[a], Eric C. Klawiter[c], Susie Y. Huang[a,d,*]

[a] Athinoula A. Martinos Center for Biomedical Imaging, Department of Radiology, Massachusetts General Hospital, Harvard Medical School, Boston, MA, USA
[b] Department of Radiology, Faculty of Medicine, Siriraj Hospital, Mahidol University, Thailand
[c] Department of Neurology, Massachusetts General Hospital, Harvard Medical School, Boston, MA, USA
[d] Harvard-MIT Division of Health Sciences and Technology, Massachusetts Institute of Technology, Cambridge, MA, USA

ARTICLE INFO

Keywords:
Multiple sclerosis
Optic radiation
Diffusion tractography
Optical coherence tomography
White matter tract integrity
Retinal thinning

ABSTRACT

Introduction: White matter damage in the visual pathway is common in multiple sclerosis (MS) and is associated with retinal thinning, although the underlying mechanism of association remains unclear. The goal of this work was to evaluate the presence and extent of white matter tract integrity (WMTI) alterations in the optic radiation (OR) in people with MS and to investigate the association between WMTI metrics and retinal thinning in the eyes of MS patients without a history of optic neuritis (ON) as measured by optical coherence tomography (OCT). We hypothesized that WMTI metrics would reflect axonal damage that occurs in the OR in MS, and that axonal alterations revealed by WMTI would be associated with retinal thinning.

Methods: Twenty-nine MS patients without previous ON in at least one eye and twenty-nine age-matched healthy controls (HC) were scanned on a dedicated high-gradient 3-Tesla MRI scanner with 300 mT/m maximum gradient strength using a multi-shell diffusion MRI protocol (b = 800, 1500, 2400 s/mm^2). The patients were divided into two subgroups according to history without ON (N = 18) or with ON in one eye (N = 11). Diffusion tensor imaging (DTI) metrics and WMTI metrics derived from diffusion kurtosis imaging were assessed in normal-appearing white matter (NAWM) of the OR and in focal lesions. Retinal thickness in the eyes of MS patients was measured by OCT. Student's t-test was used to assess group differences between MRI metrics. Linear regression was used to study the relationship between OCT metrics, including retinal nerve fiber layer (RNFL) and combined ganglion cell and inner plexiform layer thickness (GCL/IPL), visual acuity measures and DTI and WMTI metrics.

Results: OR NAWM in MS showed significantly decreased axonal water fraction (AWF) compared to HC (0.36 vs 0.39, $p < 0.001$), with similar trends observed in AWF of lesions compared to NAWM (0.27 vs 0.36, $p < 0.001$). Fractional anisotropy (FA) was lower in OR NAWM of MS patients compared to HC (0.49 vs 0.52, $p < 0.001$). In patients without ON, AWF was the only diffusion MRI metric that was significantly associated with average RNFL ($r = 0.68$, $p = 0.005$), adjusting for age, sex and disease duration and correcting for multiple comparisons. Of all the DTI and WMTI metrics, AWF was the strongest and most significant predictor of average RNFL thickness in MS patients without ON. There was no significant correlation between visual acuity scores and DTI or WMTI metrics after correction for multiple comparisons.

Conclusion: Axonal damage may be the substrate of previously observed DTI alterations in the OR, as supported by the significant reduction in AWF within both NAWM and lesions of the OR in MS. Our results support the concept that axonal damage is widespread throughout the visual pathway in MS and may be mediated through trans-synaptic degeneration.

1. Introduction

Multiple sclerosis (MS) is the most common chronic inflammatory disorder of the central nervous system (Compston and Coles, 2008), and visual dysfunction is a common clinical manifestation (Balcer, 2006). MS lesions involving the pre- and post-chiasmatic optic pathway,

* Correspondence author at: Department of Radiology, Massachusetts General Hospital, 149 13th Street, Room 2301, Charlestown, MA 02129, USA.
E-mail address: susie.huang@mgh.harvard.edu (S.Y. Huang).

https://doi.org/10.1016/j.nicl.2020.102293
Received 4 February 2020; Received in revised form 23 April 2020; Accepted 17 May 2020
Available online 26 May 2020

including the optic radiations (OR), appear hyperintense on conventional T2-weighted and fluid attenuation inversion recovery (FLAIR) magnetic resonance imaging (MRI); however, abnormalities are known to exist in the normal appearing white matter (NAWM) that are not well demonstrated on routine structural imaging.

MS is associated with retinal thinning independent of a history of optic neuritis (Oberwahrenbrock et al., 2012), which can be interrogated precisely using optical coherence tomography (OCT). OCT, a non-invasive imaging test using light waves to measure nonmyelinated CNS axons in the retina (Zimmermann et al., 2013), has demonstrated promise as an accessible tool to evaluate retinal structures in MS (Sepulcre et al., 2007). Specifically, the retinal nerve fiber layer (RNFL) is composed of unmyelinated axons of the retinal ganglion cells that form the optic nerve and has been proposed as a surrogate biomarker of axonal damage in MS (Sepulcre et al., 2007; Toledo et al., 2008).

Diffusion MRI is sensitive to microstructural changes in white matter even without detectable lesions on routine structural imaging. Previous studies using diffusion tensor imaging (DTI) to evaluate white matter damage at the voxel level in the OR including lesions and NAWM have shown a significant decrease in fractional anisotropy (FA) and increase in radial diffusivity (RD) correlating with retinal thinning (Alves et al., 2018; Balk et al., 2015; Klistorner et al., 2014; Rocca et al., 2013) and worsening visual function in MS (Reich et al., 2009). Despite the promise of DTI in evaluating pathological change in the visual pathway, DTI metrics such as FA and RD are affected by multiple factors including demyelination (Schmierer et al., 2007), axonal loss (Klawiter et al., 2011) and fiber dispersion, suggesting the need for imaging markers with greater specificity to axonal damage in the visual pathway.

Advanced multi-compartment diffusion MR methods have been developed and proposed as more specific markers for axonal damage than DTI metrics. White matter tract integrity (WMTI) is an advanced diffusion model based on diffusion kurtosis imaging (DKI) that evaluates white matter integrity through quantification of axonal water fraction (AWF), intra-axonal diffusivity (Da), radial diffusivity of the extra-axonal space (De,perp), axial diffusivity of the extra-axonal space (De,||), and tortuosity of the extra-axonal space (Tort) (Fieremans et al., 2011; Veraart et al., 2013). WMTI accounts for the additional contribution of non-Gaussian diffusion that is present in white matter as a result of microstructural complexity (Jensen and Helpern, 2010; Jensen et al., 2005) and may improve the characterization of subtle tissue microstructural changes in demyelinating diseases such as MS.

The goal of this study was to determine the presence and extent of changes in WMTI metrics in the NAWM of the OR of people with MS and to investigate the association between these advanced diffusion MRI metrics and retinal thinning as measured by OCT in the eyes of people with MS without a history of involvement by optic neuritis. We hypothesized that WMTI metrics would reflect the axonal damage that occurs in the NAWM of the OR in MS, and that axonal alterations revealed by WMTI would be associated with retinal thinning and visual dysfunction.

2. Methods

2.1. Participants

Twenty-nine people with MS were recruited from the Massachusetts General Hospital MS Clinic between 2015 and 2019. Inclusion criteria for MS patients were: a diagnosis of clinically definite MS, absence of clinical relapse within 3 months, and being on stable disease-modifying treatment or no treatment for at least 6 months. Exclusion criteria were: systemic or ocular disease other than optic neuritis, history of optic neuritis (ON) involving both eyes, severe claustrophobia, presence of non-MRI compatible implants/devices, and other contraindications to MRI. Twenty-nine age-matched HCs were recruited for MRI only.

3. Visual acuity assessment

Visual acuity was measured in the MS patients using high-contrast (100%) and low-contrast (2.5% and 1.25%) letter acuity Sloan charts, viewed from two meters away in a well-lit room. The number of correctly identified letters (maximum 60/chart) was recorded for each eye.

4. Disability assessment

A board- and Expanded Disability Status Scale (EDSS)-certified neurologist blinded to imaging and OCT data conducted a standard clinical examination for each MS patient, which was used in the calculation of the EDSS.

5. Optic nerve lesions

To assess for the presence of subclinical optic neuritis (London et al., 2019), a systematic review of the available medical records and clinical MRIs of all patients was performed by a neuroradiologist. We searched for a history of transient visual loss, signs of visual dysfunction on the neurological exam, and presence of optic nerve lesions on T2/FLAIR imaging of the brain and optic nerves, among other factors that could indicate a prior episode of optic neuritis not documented in the study records.

6. Optical coherence tomography

For each MS patient, spectral domain OCT was conducted within 30 days of the MRI scan using a Zeiss Cirrus HD-OCT (model 4000–4648, software version 7.0.3.19). Scans acquired in both eyes were Macular Cube Scan 512 × 128 and Optic Disc Cube 200 × 200. OCT data were acquired in a dark room, and a minimum signal strength of 7 was required for each scan. Average, nasal and temporal quadrant RNFL and GCL/IPL were measured. Our OCT scans fulfilled OSCAR-IB quality control criteria.

7. MRI acquisition

All subjects were scanned using a multi-shell diffusion imaging protocol on a dedicated high-gradient 3-Tesla MRI scanner (MAGNETOM CONNECTOM, Siemens Healthineers, Erlangen, Germany) equipped with 300 mT/m maximum gradient strength (McNab et al., 2013; Setsompop et al., 2013; Fan et al., 2018; Huang et al., 2015, 2016). A custom-made 64-channel phased array head coil was used for signal reception (Keil et al., 2013). Diffusion data were acquired at 2 mm isotropic resolution using a single-refocused diffusion-weighted pulsed-gradient spin-echo echo planar imaging sequence with the following parameters: repetition time (TR) = 3800 ms, echo time (TE) = 77 ms, generalized auto-calibrating partially parallel acquisition (GRAPPA) factor = 2, simultaneous multislice (SMS) factor = 2, anterior-to-posterior phase encoding, b = 800, 1500, 2400 s/mm^2, 32 uniformly distributed directions for b < 2000 s/mm^2 and 64 uniformly distributed directions for b > 2000 s/mm^2 (Huang et al., 2019, 2020; Fan et al., 2019). b = 0 images were interspersed for every 16 diffusion-weighted images. A set of 5 b = 0 images with reversal of the phase-encoding direction (posterior to anterior) was acquired separately to correct for geometric distortions due to susceptibility effects.

Structural imaging included a high-resolution three-dimensional T1-weighted (T1w) multi-echo magnetization-prepared rapid gradient echo (MEMPRAGE) sequence [TR/TE = 2530/[1.15, 3.03, 4.89, 6.75] ms, inversion time (TI) = 1100 ms, 1 × 1 × 1 mm^3 voxels, R = 2] and three-dimensional fluid-attenuated inversion recovery (FLAIR) images [TE/TR/TI = 389/5000/1800 ms, 0.9 × 0.9 × 0.9 mm^3 voxels, R = 2]. The structural images were used for registration and segmentation.

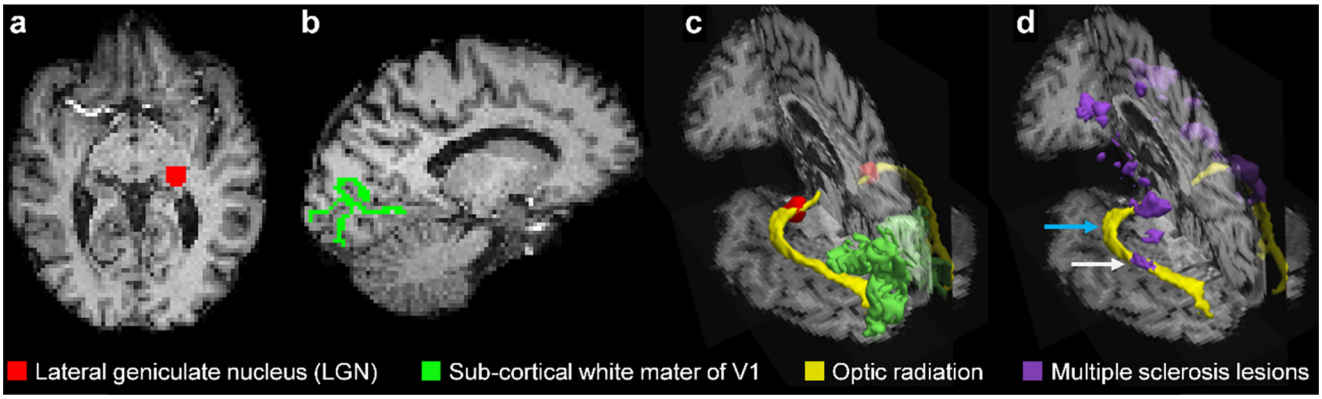

Fig. 1. Diffusion tractography results of the optic radiation (OR) in a representative MS patient. (a) Lateral geniculate nucleus (LGN) region-of-interest (ROI). (b) Subcortical white matter of the primary visual cortex (V1) ROI. (c) Volume-rendered thresholded probabilistic tractography results for the OR (yellow), LGN ROI (red) and V1 ROI (green). (d) Volume-rendered thresholded probabilistic tractography results for the OR (yellow) with segmented MS lesions (purple). The white arrow highlights the MS lesion in the OR while the blue arrow highlights the normal appearing white matter of the OR. (For interpretation of the references to colour in this figure legend, the reader is referred to the web version of this article.)

8. Data processing

The diffusion data and antomical data were preprocessed using the pipeline established for the MGH-USC Human Connectome project (Fan et al., 2016). In brief, all images were first corrected for gradient nonlinearity distortion using in-house developed MATLAB tools. The diffusion data was corrected for susceptibility- and eddy current-induced distortions using the TOPUP (Andersson et al., 2003) and EDDY (Andersson et al., 2016; Andersson and Sotiropoulos, 2016) functions in the FMRIB Software Library (FSL, https://fsl.fmrib.ox.ac.uk) (Smith et al., 2004). Cortical surface reconstruction and volumetric segmentation was performed on the T1w images of all subjects using FreeSurfer software (version 6.0, https://surfer.nmr.mgh.harvard.edu) (Dale et al., 1999). The averaged $b = 0$ images were co-registered to the T1w images using the boundary-based registration using the "bbregister" function in FreeSurfer (Greve and Fischl, 2009).

9. Regions of interest

Regions-of-interest (ROIs) for diffusion tractography were generated from FreeSurfer reconstruction results. ROIs corresponding to the lateral geniculate nucleus (LGN) and the sub-cortical white matter of the primary visual cortex (V1) were generated as follows. The LGN ROI was derived from the segmentation provided by a recently implemented tool built into FreeSurfer using a probabilistic atlas of the human thalamic nuclei that combines ex vivo MRI and histology (Iglesias et al., 2018). The LGN ROI was converted into a binary mask and transformed to diffusion image space. The ROI for the sub-cortical white matter of V1 was generated using the V1 surface label for each hemisphere derived from Freesurfer (V1_exvivo.thresh.label from 'fsaverage' (Fischl et al., 2008)). The V1 surface label was converted into a binary mask in diffusion space and sampled as a 1 mm ribbon of subcortical white matter deep to the gray-white surface. The 1 mm ribbon of subcortical white matter in V1 was chosen as the target ROI for tractography in order to capture as many fibers as possible emanating from the LGN and extending to the gray-white surface, while excluding any fibers that could potentially extend into the gray matter. Binary masks of the corpus callosum were also extracted from the FreeSurfer white matter parcellation to serve as exclusion masks for tractography.

In addition to extracting ROIs for diffusion tractography, we also derived estimates of cortical thickness and volume for ROIs of primary and secondary visual cortex, V1 and V2, defined by the Desikan-Killiany atlas provided in FreeSurfer (Desikan et al., 2006). The volume of the LGN was derived from the built-in segmentation tool for human thalamic nuclei in FreeSurfer as described above (Iglesias et al., 2018).

10. Diffusion tractography

10.1. Optic radiations

We produced binarized masks of the bilateral OR based on thresholded probabilistic tractography, tracking from LGN to ipsilateral V1 and V1 to LGN with inclusion of Meyer's loop as part of the OR, following the procedure described below. Voxel-wise crossing fiber orientation distributions were estimated for probabilistic tractography using the "bedpostx" function in FSL. The $b = 800$, 1500, and 2400 s/mm^2 data were used for "bedpostx" fitting using the multi-shell option, assuming a two-stick model and Rician noise. To obtain more robust tractography results, probabilistic tractography was performed using the "probtrackx2" function in FSL (Behrens et al., 2007) in two directions: 1) LGN to ipsilateral V1, with the LGN as the "seed" and the ipsilateral subcortical V1 as the "target"; 2) V1 to LGN, with the subcortical V1 as the "seed" and the ipsilateral LGN as the "target." The corpus callosum mask generated from the FreeSurfer label for the corpus callosum served as the exclusion mask. 5000 streamlines were generated from each voxel in the seed ROI, and only those streamlines that passed through the ipsilateral target ROI, and not entering the exclusion mask, were retained. The tractography results acquired between LGN to subcortical V1 and subcortical V1 to LGN were averaged to generate a robust tractography result. The tractography results were then normalized by the total number of streamlines between the whole seed region and the target region (called "waytotal" number), so that a given threshold could be set for choosing the voxels belonging to the optic radiation across all subjects. To ensure that the tractography results would not be biased in the presence of lesions, we used a threshold of 1% for binarizing the probabilistic tractography results into a mask and for volume rendering of the tractography results. The threshold of 1% was set empirically to ensure that voxels within lesions were not excluded from the OR masks (Supplementary Fig. 1). Fig. 1 shows an example of the probabilistic tractography results in a representative MS patient.

11. Corticospinal tracts

To assess the specificity of the diffusion MRI findings to the visual pathway, ROIs of the corticospinal tracts were generated for each patient without a history of ON based on the HCP1065 standard-space DTI templates derived from 1065 Human Connectome Project subjects (https://fsl.fmrib.ox.ac.uk/fsl/fslwiki/Atlases). The FA map for each subject was nonlinearly registered to the template FA map using FNIRT (https://fsl.fmrib.ox.ac.uk/fsl/fslwiki/FNIRT). The inverse

transformation was then applied to the binary tract ROIs derived from the HCP1065 atlas, which were created by thresholding the template probabilistic tractography maps at 90%. The binarized masks of the bilateral corticospinal tracts were used to calculate ROI-based statistics of diffusion metrics in the corticospinal tracts.

12. Lesion and normal-appearing white matter segmentation

Lesion segmentation was performed on the 3D FLAIR images of all MS patients. The FLAIR images were first registered to the T1w data using the boundary-based registration tool in FreeSurfer. Automatic segmentation of FLAIR hyperintense lesions was then performed using a FreeSurfer-based validated tool that uses T1w and FLAIR images as inputs (Lindemer et al., 2015; Yu et al., 2019). The lesion masks were then manually edited by a board- and subspecialty-certified neuroradiologist (C.N.). The lesion masks were subtracted from the OR masks to generate NAWM masks within the OR and from the corticospinal tract ROIs to generate NAWM masks within the corticospinal tracts. The lesion and NAWM masks within the OR were systematically checked against the FLAIR images after each processing step to ensure that the masks aligned well with the lesions and NAWM seen on the FLAIR images. The lesion volume in the OR was also calculated. Averaged lesion volume between the left and right side was used for subsequent analyses.

13. Diffusion metrics

The diffusion tensor model was fitted on the pre-processed diffusion MRI $b = 800$ s/mm^2 data using the "dtifit" function in FSL to derive maps of fractional anisotropy (FA), mean diffusivity (MD), axial diffusivity (AD) and radial diffusivity (RD). Mean values of FA, MD, AD and RD were extracted from ROIs comprising the reconstructed OR in each subject.

We used the DKI fitting tool from https://github.com/NYU-DiffusionMRI/Diffusion-Kurtosis-Imaging for deriving the WMTI metrics. Based on the biophysical diffusion model that separates the white matter into myelin, intra- and extra-axonal spaces and estimation of diffusion and kurtosis model parameters including WMTI, using diffusion kurtosis imaging, the axonal water fraction (AWF), intra-axonal diffusivity (Da), radial and axial extra-axonal diffusivity (De,perp and De,||) and tortuosity (Tort) were calculated and reported (Fieremans et al., 2011; Veraart et al., 2013). We quantified 1) axonal water fraction (AWF), which represents the ratio of water in the intra-axonal space over the total amount of water and represents axonal loss; 2) the intra-axonal diffusivity (Da), which represents the water diffusivity in the axons and is a potential marker of intra-axonal injury; 3) radial extra-axonal diffusivity (De,perp), which is sensitive to the degree of demyelination and increases in the presence of extensive demyelination; 4) axial extra-axonal diffusivity (De,||); 5) and tortuosity of the extra-axonal space (Tort), defined as the ratio of axial extra-axonal diffusivity to the perpendicular extra-axonal diffusivity (De,||/De,perp), which is presumed to be a marker of demyelination (Fieremans et al., 2011; Veraart et al., 2013).

13.1. Statistical analysis

Diffusion metrics in the bilateral OR were averaged for subsequent analyses (Tur et al., 2016). For patients with a history of optic neuritis in only one eye (MS_ON), the OCT data from the eye not affected by optic neuritis and diffusion metrics averaged in the bilateral OR were used. For patients with no history of optic neuritis (MS_NON), the average of the OCT data from both eyes and diffusion metrics averaged in the bilateral OR were used for further analyses. Our patients were divided on the subject level into patients without history of optic neuritis in either eye (MS_NON) and with a history of optic neuritis (MS_ON) in one eye.

All statistical calculations were all performed in MATLAB software version 9.4 (MathWorks, Natick, Massachusetts). The Shapiro-Wilk test was used to assess normality of the data. Student's t-tests, Wilcoxon rank-sum test and chi-square tests were used as indicated to evaluate differences in demographic and clinical variables, lesion volumes and diffusion metrics between MS patients with HCs and between MS_NON and MS_ON patients, and to compare OCT data among MS patients. Specifically, we compared the average RNFL and GCL + IPL in the NON eyes of MS_ON and MS_NON using Student's t-tests. The average RNFL and GCA + IPL between the left and right eyes in MS_NON were also compared using Student's t-tests.

Individual correlations between OCT data as well as visual acuity scores and the diffusion metrics of FA, MD, AD, RD, AWF, De,perp, De,||, and tortuosity were assessed adjusting for age, sex and disease duration as factors that could influence microstructural metrics in the optic radiation. A multiple linear regression model that included terms for FA, AWF and sex as predictors was used to assess the relative contribution in predicting OCT metrics.

For the tract-specific analyses, the associations between diffusion MRI measures in the bilateral corticospinal tracts and retinal thinning were assessed using Pearson partial correlation, adjusting for age, sex and disease duration. For the sensitivity analyses, the associations between diffusion MRI measures in the right and left portions of the OR separately and retinal thinning were tested using Pearson partial correlation, adjusting for age, sex and disease duration. The associations between cortical thickness and volume of primary and secondary visual cortex, V1 and V2, and LGN volume with retinal atrophy were tested using Pearson partial correlation, adjusting for age, sex and disease duration.

Based on an earlier study showing that severe optic nerve damage might mask or interfere with the relationship between the OR and visual function (Reich et al., 2009), we studied the association between diffusion metrics in the OR NAWM and visual acuity in patients with average RNFL $>$ 80 μm.

For all statistical analyses, corrections for multiple comparison were conducted based on false discovery rate (FDR) adjustment with an FDR threshold of 0.05. The raw uncorrected p-values surviving FDR correction are reported here.

14. Results

Clinical and demographic data for the MS patients and HC are presented in Table 1. There was no significant difference in age or sex between the HC and MS groups ($p = 0.14$ and $p = 0.39$, respectively). Of the 29 MS patients, 18 had no previous history of optic neuritis (MS_NON), and 11 had experienced optic neuritis in one eye (MS_ON, left eye = 6, right eye = 5). Patients with a history of optic neuritis in one eye were slightly younger than patients with no previous history of optic neuritis, but the difference was not statistically significant. No asymptomatic optic nerve lesions were found in the NON-eyes of any patients.

No significant difference in average RNFL and GCL + IPL was observed in the NON eyes of MS_ON and MS_NON (average RNFL of NON eyes of MS_ON versus MS_NON = 92.17 vs. 91.66, $p = 0.93$; average GCA + IPL of NON eyes of MS_ON versus MS_NON = 76.55 vs. 80.36, $p = 0.39$). In addition, there was no significant difference in the average RNFL or GCA + IPL between the left and right eyes in MS_NON (average RNFL, $p = 0.16$ and GCA + IPL, $p = 0.25$), in keeping with the bilateral nature of retinal thinning previously reported in MS patients without a history of optic neuritis (Klistorner et al., 2014).

Greater RNFL thickness (average, nasal and temporal quadrants) and thicker GCL + IPL were significantly associated with better low-contrast visual acuity (LCVA at 1.25%) in the MS group as a whole ($r = 0.44$, $p = 0.031$; $r = 0.43$, $p = 0.034$; $r = 0.49$, $p = 0.01$ and $r = 0.48$, $p = 0.02$, respectively). These results confirmed that the OCT data mirrored visual function assessment (Klistorner et al., 2014; Reich

Table 1
Demographic and clinical information for healthy control subjects and multiple sclerosis patients.

	HC (n = 29)	MS (n = 29)	MS_NON (n = 18)	MS_ON (n = 11)	p-value (MS_NON vs MS_ON)
Age (Y), mean ± SD [range]	41.72 ± 13.4 [23–69]	42.83 ± 11.7 [23–68]	45.94 ± 9.7 [29–68]	37.73 ± 13.3 [23–58]	0.07[1]
Sex (M/F)	11/18	7/22	6/12	1/10	0.30[2]
Disease duration (Y), mean ± SD [range]	NA	8.66 ± 6.7 [2–24]	9.1 ± 6.5 [2–24]	7.91 ± 7.3 [2–23]	0.65[1]
MS subtype (RRMS/SPMS)	NA	24/5	16/2	8/3	0.54[2]
Disease-modifying therapy, n (%), RRMS/SPMS		27 (93.1%), 24/3	17 (94.4%), 16/1	10 (90.9%), 8/2	0.69[2]
Dimethyl fumarate		8 (27.6%), 8/0	4 (22.2%), 4/0	4 (36.4%), 4/0	
Glatiramer acetate		7 (24.1%), 7/0	5 (27.8%), 5/0	2 (18.2%), 2/0	
β-interferons		1 (3.4%), 1/0	0	1 (9.1%), 1/0	
Fingolimod		4 (13.8%), 3/1	4 (22.2%), 3/1	0	
Natalizumab		2 (6.9%), 2/0	1 (5.6%), 1/0	1 (9.1%), 1/0	
Rituximab		2 (6.9%), 0/2	0	2 (18.2%), 0/2	
Ocrelizumab		3 (10.3%), 3/0	3 (16.7%), 3/0	0	
None		2 (6.9%), 0/2	1 (5.6%), 0/1	1 (9.1%), 0/1	
EDSS score, mean ± SD, median [range]	NA	2.83 ± 1.82, 2.0 [1.0–6.5]	2.75 ± 1.48, 2.5 [1.0–6.5]	2.95 ± 2.39, 2.0 [1.0–6.5]	0.51[3]
Mean RNFL, mean ± SD [range]	NA	91.85 ± 14.93 [60.5–124.3]	91.66 ± 13.78 [70.4–120]	92.17 ± 17.4 [60.5–124.3]	0.93[1]
Mean GCL + IPL, mean ± SD [range]	NA	78.91 ± 11.32 [45–95]	80.36 ± 9.1 [62.5–94]	76.55 ± 14.4 [45–95]	0.39[1]
Mean letter acuity score at 100% contrast, mean ± SD [range]	NA	51.3 ± 9.7 [21–60]	53.28 ± 5.4 [45–60]	48.45 ± 13.7 [21–60]	0.21[1]
Mean letter acuity score at 2.5% contrast, mean ± SD [range]	NA	26.3 ± 11.4 [0–44]	28.84 ± 10.8 [4.5–44]	26.91 ± 12.7 [0–43]	0.82[1]
Mean letter acuity score at 1.25% contrast, mean ± SD [range]	NA	7.3 ± 8.6 [0–25]	3.53 ± 4.8 [0–14]	12.7 ± 10.3 [0–25]	0.02[3]

Note. – EDSS = Expanded Disability Status Scale, NA = not applicable, RNFL = retinal nerve fiber layer thickness, GCL + IPL = ganglion cell layer thickness (GCL) combined with the inner plexiform layer (IPL). RNFL and GCL + IPL are reported in microns.
[1] Student's *t*-test.
[2] Chi-Square Test.
[3] Wilcoxon rank-sum test.

et al., 2009) (Balcer et al., 2017). A significant correlation was also observed between the RNFL thickness (average and temporal RNFL) and EDSS ($r = -0.4$, $p = 0.046$ and $r = -0.46$, $p = 0.017$), consistent with previous reports (Toledo et al., 2008) (Sepulcre et al., 2007).

All MS subjects had T2/FLAIR hyperintense brain lesions. The average volume of brain lesions among the MS patients was 4494 mm^3. Twenty-two MS patients had lesions in the OR, including 13 patients in the MS_NON subgroup and 9 patients in the MS_ON subgroup. The average OR lesion volume was 123.9 mm^3. A high degree of correlation was observed between brain lesion volume and OR lesion volume among all MS patients ($r = 0.84$, $p < 0.0001$), confirming that lesion load in the OR reflected the overall burden of disease (Klistorner et al., 2014).

The OR ROIs and diffusion metric maps were successfully reconstructed in all subjects. Optic radiation NAWM of MS patients showed significantly decreased FA, AWF and Tort and increased MD, RD and De,perp compared to HCs, with similar trends seen in MS lesions compared to NAWM in MS, including increased AD in MS lesions (Table 2). Comparison of the OR NAWM diffusion metrics between the MS_NON and MS_ON subgroups showed trends toward decreased FA, AWF and increased MD and RD in patients with ON involving one eye versus patients without a history of ON (Supplementary Table 1).

15. Subgroup analysis of patients without history of ON

In order to exclude the potential contribution of the ON eye on diffusion MRI metrics in the OR, we performed subgroup analyses focusing on the relationship between the OCT and diffusion MRI measures in (a) patients without a previous history of ON (MS_NON, N = 18) and (b) patients with a history of ON involving one eye (MS_ON, N = 11). In the MS_NON group, AWF was the only diffusion MRI metric that was significantly associated with average RNFL ($r = 0.68$, $p = 0.005$), adjusting for age, sex and disease duration and correcting for multiple comparisons (Table 3). In the MS_ON group, there was no significant relationship between any diffusion metric in the OR NAWM and the OCT metrics of average, nasal and temporal RNFL and GCL + IPL in the non-optic neuritis eye, after correcting for multiple comparisons and adjusting for age, sex, disease duration and the corresponding OCT data from the ON (affected) eye (Supplementary Table 2).

Given the small sample size of the MS_NON group, we performed a sensitivity analysis using the right and left portions of the OR separately to increase power in one region and decrease it in the other due to the even distribution of lesions in both OR. We found significant correlations between AWF in the right OR with average RNFL ($r = 0.60$, $p = 0.02$) and between FA and AWF in the left OR with average RNFL (FA, $r = 0.63$, $p = 0.01$; AWF, $r = 0.73$, $p = 0.002$).

To determine the relative contribution of the DTI and WMTI metrics in explaining the degree of retinal thinning as measured by OCT, a multiple linear regression model was constructed that included terms for FA, AWF and sex as predictors of the OCT data in the MS_NON subgroup. AWF in the OR NAWM was the only measure that was significantly associated with average RNFL ($b = 339.63$, $p = 0.03$).

To help clarify the tract specificity of the association between diffusion MRI metrics in the OR and retinal thinning in the MS_NON subgroup, we studied the association between the OCT data and diffusion MRI measures in a separate major white matter tract outside the visual pathway, the corticospinal tract. FA of the NAWM of the corticospinal tract was significantly associated with temporal RNFL ($r = -0.76$, $p = 0.0009$), but not AWF ($r = -0.24$, $p = 0.39$).

No significant correlations were found between the diffusion metrics in the OR NAWM and visual acuity measures in the MS group as a whole (Table 4), nor within the MS_NON and MS_ON subgroups (Supplementary Table 3 and 4).

In addition to studying the effects of OR damage in the retina by diffusion MRI, we evaluated the relationships between retinal thickness

Table 2
Comparison of the OR diffusion metrics between HCs and MS patients.

Diffusion MR metrics	HC	MS		p-value	
		NAWM	Lesion	HC vs NAWM	NAWM vs Lesion
DTI					
FA	0.52 (0.02)	0.49 (0.041)	0.36 (0.08)	< 0.001*	< 0.001*
MD ($\times 10^{-3}$)	0.91 (0.04)	1.01 (0.19)	1.26 (0.19)	0.014*	< 0.001*
AD ($\times 10^{-3}$)	1.50 (0.06)	1.59 (0.29)	1.76 (0.24)	0.1	0.03*
RD ($\times 10^{-3}$)	0.61 (0.04)	0.71 (0.16)	1.00 (0.19)	0.003*	< 0.001*
WMTI					
AWF	0.39 (0.02)	0.36 (0.03)	0.27 (0.03)	< 0.001*	< 0.001*
Da	1.05 (0.06)	1.04 (0.06)	0.99 (0.17)	0.7	0.13
De, perp	1.03 (0.05)	1.09 (0.14)	1.4 (0.28)	0.02*	< 0.001*
De, ||	2.36 (0.09)	2.36 (0.19)	2.44 (0.38)	0.9	0.4
Tort	2.48 (0.17)	2.33 (0.21)	1.77 (0.29)	0.004*	< 0.001*

Note. – Diffusion metric differences between MS from HCs were assessed using Student's t tests. Mean values are reported with standard deviations shown in parentheses.

* Denotes significance following correction for multiple comparisons (FDR threshold of 0.05). Raw p-values are reported in the table.

Table 3
Correlation between diffusion metrics in OR NAWM and OCT data in patients with no previous history of optic neuritis (MS_NON, N = 18).

Diffusion metrics	Average RNFL	Nasal RNFL	Temporal RNFL	GCL + IPL
DTI				
FA	0.55 (0.03)	0.45 (0.09)	0.37 (0.18)	0.39 (0.15)
MD	−0.48 (0.07)	−0.2 (0.46)	−0.57 (0.03)	−0.39 (0.15)
AD	−0.27 (0.34)	0.03 (0.9)	−0.51 (0.05)	−0.27 (0.33)
RD	−0.54 (0.037)	−0.3 (0.26)	−0.55 (0.035)	−0.4 (0.1)
WMTI				
AWF	0.68 (0.005)*	0.52 (0.046)	0.47 (0.08)	0.52 (0.048)
Da	0.5 (0.057)	0.47 (0.07)	0.19 (0.5)	0.24 (0.39)
De, perp	−0.2 (0.47)	−0.04 (0.9)	−0.36 (0.2)	−0.03 (0.9)
De, ||	0.39 (0.15)	0.54 (0.038)	−0.06 (0.8)	0.3 (0.23)
Tort	0.42 (0.12)	0.38 (0.16)	0.29 (0.29)	0.23 (0.4)

Note. – Correlation analysis using weighted Pearson partial correlation coefficients controlled for age, sex and disease duration. Raw p-values are shown in parentheses. *denotes significant correlations following correction for multiple comparisons (FDR threshold of 0.05).

Table 4
Correlation analysis between diffusion metrics in OR NAWM and visual acuity scores at 100%, 2.5%, and 1.25% contrast for MS patients.

Diffusion metrics	VA at 100% contrast	VA at 2.5% contrast	VA at 1.25% contrast
DTI			
FA	−0.2 (0.4)	−0.1 (0.6)	−0.14 (0.56)
MD	−0.04 (0.9)	0.197 (0.42)	0.53 (0.018)
AD	−0.08 (0.7)	0.199 (0.41)	0.55 (0.01)
RD	0.002 (0.99)	0.191 (0.43)	0.5 (0.03)
WMTI			
AWF	−0.1 (0.6)	−0.019 (0.9)	−0.24 (0.33)
Da	−0.2 (0.4)	−0.076 (0.76)	0.32 (0.18)
De, perp	0.13 (0.6)	0.21 (0.38)	0.33 (0.16)
De, ||	0.03 (0.9)	0.29 (0.23)	0.54 (0.02)
Tort	−0.1 (0.6)	−0.082 (0.74)	0.02 (0.93)

Note. – Correlation analysis using Pearson partial correlation coefficients adjusting for age, sex and disease duration (p-values are shown in parentheses). Only cases with RNFL thickness > 80 μm (N = 22) were included in the analysis.

*Denotes significance following correction for multiple comparisons (FDR threshold of 0.05). Raw p-values are reported in the table.

and regional cortical thickness and volume of primary and secondary visual cortex, V1 and V2, as well as the volume of the LGN. For all MS subjects (N = 29), thinning of the RNFL was significantly associated with lower cortical volume in V1 and V2 (r = 0.46, p = 0.02 and r = 0.44, p = 0.02, respectively). Also, thinning of the GCL + IPL was significantly associated with lower cortical volume and thickness in V2 (r = 0.50, p = 0.01 and r = 0.46, p = 0.02, respectively). Thinning of the average and temporal RNFL and GCL + IPL was significantly associated with lower LGN volume (r = 0.57, p = 0.002; r = 0.59, p = 0.001 and r = 0.60, p = 0.001, respectively). For MS_NON subgroup (N = 18), the result showed trends of relationship between thinning of average RNFL and GCL + IPL with lower V1 volume (r = 0.55, p = 0.03 and r = 0.53, p = 0.04, respectively) as well as significant correlation between thinning of temporal RNFL and GCL + IPL with lower LGN volume (r = 0.7, p = 0.003 and r = 0.66, p = 0.008, respectively).

16. Discussion

In this study, we evaluated WMTI metrics as derived from DKI in the OR NAWM of people with MS as potential biomarkers of axonal damage in the posterior visual pathway, and assessed the relationship of these metrics with retinal thinning in MS. Our results showed significantly reduced AWF and tortuosity in the OR NAWM of people with MS compared to the OR of HCs, with similar alterations in lesions compared to the OR NAWM. Furthermore, a strong and significant association was observed between lower AWF in the OR and thinning of the average RNFL in patients without a history of ON. Of all the DTI and WMTI metrics, AWF was the strongest and most significant predictor of average RNFL thickness in MS patients without ON.

AWF represents the ratio of water within the intra-axonal space over the total amount of water in the intra- and extra-axonal space, neglecting the contribution of myelin water (Fieremans et al., 2011). AWF is thought to reflect chronic axonal degeneration and loss in MS (de Kouchkovsky et al., 2016) and may offer greater pathologic specificity

to axonal loss and damage than DTI metrics (Chung et al., 2018; Fieremans et al., 2013; Margoni et al., 2019). The observed decrease in AWF suggests tissue damage in the OR, which we show to be significantly correlated with axonal thinning of the retinal ganglion cells in patients without ON. Our findings are consistent with previous studies showing a close relationship between RNFL thinning and DTI metrics (Klistorner et al., 2014) and provide further evidence linking axonal damage of the OR white matter and retinal thinning in MS.

In this study, we excluded eyes that were affected by optic neuritis in order to study the relationship between DTI metrics in the OR NAWM and retinal thinning selectively, unconfounded by prior involvement by optic neuritis. Thinning of the RNFL in patients with MS without a history of ON (MS-NON) has been reported (Klistorner et al., 2014; Sepulcre et al., 2007). However, the pathologic basis for this thinning remains unclear. Several mechanisms including subclinical inflammation of the optic nerve, primary retinal pathology, and retrograde trans-synaptic degeneration have been suggested. The strong association between OR AWF and retinal thinning as measured by the average RNFL thickness in patients without a history of ON supports a tract-specific association between axonal damage in the OR and thinning of the retinal ganglion cell axons.

AWF in the normal-appearing corticospinal tract of patients without a history of ON did not significantly correlate with either RNFL or GCL + IPL, whereas FA in the normal-appearing corticospinal tract was significantly associated with temporal RNFL. Furthermore, in analyses of diffusion MRI metrics drawn from the left and right OR separately, we found significant correlations for AWF and retinal thinning in both OR but not for FA. These additional findings suggest that DTI metrics such as FA may reflect a diffuse neurodegenerative process that also influences the OCT measures, whereas DKI metrics such as AWF may be more specific for white matter tract integrity in the visual pathway.

In patients with a history of ON involving one eye, no significant relationship was observed between diffusion MRI metrics averaged across both OR and OCT data from the NON eye, which agrees with findings of previous studies that did not show a strong relationship between retinal thinning and DTI measures in patients with prior ON involving at least one eye (Alves et al., 2018). The negative findings in the MS_ON group may be related in part to the smaller sample size of the MS_ON subgroup (N = 11) compared to the MS_NON subgroup (N = 18). In addition, inclusion of fibers from the ON eye in the diffusion MRI measures could potentially mask the true retinal-white matter relationship following a prior episode of ON (Klistorner et al., 2014).

The upstream and downstream effects of retinal thinning and axonal damage on cortical atrophy in primary visual cortex and the volume of LGN are suggested by the trend toward association between decreased V1 volume with thinning of average RNFL and GCL + IPL, as well as the significant relationship between decreased LGN volume with lower temporal RNFL and GCL + IPL. Our results support the notion that axonal damage is widespread throughout the visual pathway in MS and may be mediated through trans-synaptic degeneration (Balk et al., 2015; Gabilondo et al., 2014; Klistorner et al., 2015; Rocca et al., 2013).

Low contrast visual acuity is a sensitive tool for evaluating visual function in MS (Balcer et al., 2007). However, no significant correlation was identified between visual acuity scores at 100%, 2.5% and 1.25% contrast and any of the diffusion metrics in the OR NAWM examined in our study. Previous studies that included both optic neuritis and non-optic neuritis eyes of MS patients for analysis showed that a reduction in low contrast vision (2.5%) was associated with decreased FA and increased RD in the OR, which included both NAWM and lesions (Reich et al., 2009). In comparison, our analysis was performed specifically in non-optic neuritis eyes, which may have made such relationships less discernible if the previously reported alterations in DTI metrics were driven by the presence of lesions and low contrast vision was in a narrower range between individuals in our current study. In our analysis of lesion volumes, significant correlations were observed between lesion volume in the OR of MS and low contrast visual acuity at 2.5% and 1.25%, which was in line with other studies (Klistorner et al., 2014). We hypothesize that there may be other contributing factors beyond optic radiation integrity that may influence visual function, such as the presence of cortical/juxtacortical lesions that are largely undetectable at 3 T without specialized pulse sequences and episodes of subclinical optic neuritis that are not easy to account for in studies.

A strength of our approach was the derivation of WMTI metrics using intermediate to high *b*-values (up to 2400 s/mm^2) on a dedicated 3 T scanner equipped with 300 mT/m gradients, nearly seven times higher than most clinical gradient strengths. As such, our diffusion MRI data were likely higher in signal-to-noise ratio compared to those acquired on conventional MRI scanners. Nevertheless, the use of *b*-values in a range that is accessible on most MRI scanners ensures that these measurements can be performed and reproduced using conventional hardware, attesting to the utility and feasibility of using WMTI to complement diffusion MRI measurements performed as part of routine clinical protocols.

Another strength of our approach was the application of a relatively novel and rigorous approach to reconstructing the fiber tracts of the OR. We conducted the fiber tracking by using PROBTRACKX and ROI selection via semi-automated segmentation through FreeSurfer following a recently developed method (Tian et al., 2018), which has been shown to be robust and reproducible in reconstructing fiber tracts. Previous studies have seeded ROIs in the OR from the LGN directly or from the whole thalamus using manual or automated methods (Alves et al., 2018; Balk et al., 2015; Horbruegger et al., 2019; Klistorner et al., 2014; Raz et al., 2015; Reich et al., 2009; Tur et al., 2016). However, the differences in tractography algorithms may limit direct comparisons with diffusion metrics derived from previous studies. Our tractography approach involved producing binarized masks of the OR based on thresholded probabilistic tractography, with a threshold that was set empirically to ensure that voxels within lesions were not excluded from the OR masks. In patients who had lesions in only one OR, there was no significant difference in the number of voxels included in the OR masks between both sides, which provides evidence that our tractography results were not strongly influenced by the presence of lesions.

Limitations of this study include the small sample size and heterogeneity of the patient population, which may limit the statistical significance of some results and the generalizability of the findings. The inclusion of a small number of patients with secondary progressive MS could potentially bias the results toward findings that would be more prevalent in the progressive phase of the disease. On the other hand, the small sample size implies that significant results are relevant but that negative results may be false negatives due to lack of statistical power. This limitation also applies to the results of the multiple regression models as well as the absence of correlation with visual acuity. In the multiple regression analysis, the only significant predictor of retinal thinning was AWF in patients without a history of ON and not FA. However, due to the small sample size, we cannot definitively conclude that FA is not a predictor in either patient group.

In addition, our study focused on the optic radiations as the key white matter pathway affected in MS, based on previous reports (Klistorner et al., 2014). As such, we did not study systematically the presence of lesions and diffusion metrics in the optic tracts or other segments of the posterior visual pathway, which was otherwise precluded by the small number of lesions and limited number of voxels within the optic tracts. We evaluated for subclinical optic nerve involvement in the NON eyes through a systematic review of the available medical records and clinical MRIs and did not find evidence of optic nerve lesions in the NON eyes of our patients. However, we did not evaluate for possible increased latency at visual evoked potentials as additional evidence of subclinical optic neuritis (London et al., 2019). In addition, the lack of significant differences of retinal thinning between NON eyes in MS_ON and MS_NON does not completely exclude the potential influence of optic neuritis on the unaffected eye. One

possible mechanism that would mediate this effect is expansion of a lesion from the ON eye into the optic chiasm, leading to retinal thinning in the contralateral NON eye (Klistorner et al., 2014).

Regarding the interpretation of AWF, several other pathological factors could contribute to the observed decrease in AWF beyond axonal damage/loss. AWF represents the ratio between water in the intra-axonal space and the total amount of water. Accordingly, the observed decrease in AWF could be due to a decrease in intra-axonal water (i.e., lower axonal volume) or an increase in the total amount of water from pathological processes such as active demyelination and inflammation. We sought to evaluate damage to the optic pathway outside the period of acute optic neuritis and active inflammatory change/demyelination by only including patients who did not have a clinical relapse within the past three months and who were considered clinically stable on their existing treatment regimens. These measures led us to be more confident that the changes in AWF would more likely reflect chronic axonal loss in the OR white matter rather than acute inflammation or active demyelination. However, we acknowledge that inflammation and demyelination remain potential contributors to the observed decrease in AWF. Finally, the cross-sectional design of our study was only able to show associations and not causation between retinal ganglion cell axonal thinning and altered white matter tract integrity in the optic radiations. Larger longitudinal studies will be needed to assess the exact relationship between retinal thinning and white matter damage in the OR.

17. Conclusion

We found a significant reduction in AWF within both NAWM and lesions of the OR in MS compared to healthy controls, as measured by WMTI metrics derived from DKI. Our results suggest that axonal damage may be the underlying substrate of previously observed DTI alterations in the OR. Of all the DTI and WMTI metrics, AWF was the strongest and most significant predictor of average RNFL thickness in MS patients without ON. Our results support the concept that axonal damage is widespread throughout the visual pathway in MS and may be mediated through trans-synaptic degeneration.

CRediT authorship contribution statement

Chanon Ngamsombat: Conceptualization, Methodology, Validation, Formal analysis, Writing - original draft, Writing - review & editing, Visualization. **Qiyuan Tian:** Conceptualization, Methodology, Software, Formal analysis, Writing - review & editing. **Qiuyun Fan:** Conceptualization, Methodology, Formal analysis, Investigation. **Andrew Russo:** Investigation, Data curation. **Natalya Machado:** Investigation, Data curation. **Maya Polackal:** Investigation, Data curation. **Ilena C. George:** Data curation. **Thomas Witzel:** Resources. **Eric C. Klawiter:** Conceptualization, Methodology, Resources, Writing - review & editing, Supervision. **Susie Y. Huang:** Conceptualization, Methodology, Resources, Writing - original draft, Writing - review & editing, Supervision, Project administration, Funding acquisition.

Acknowledgments

Funding provided by the National Institutes of Health (USA), grant numbers P41-EB015896, S10-RR019307, and K23-NS096056, the Conrad N. Hilton Foundation Pilot Innovator Award #17330, and an MGH Claflin Distinguished Scholar Award.

Appendix A. Supplementary data

Supplementary data to this article can be found online at https://doi.org/10.1016/j.nicl.2020.102293.

References

Alves, C., Batista, S., d'Almeida, O.C., Sousa, L., Cunha, L., Bernardes, R., Castelo-Branco, M., 2018. The retinal ganglion cell layer predicts normal-appearing white matter tract integrity in multiple sclerosis: A combined diffusion tensor imaging and optical coherence tomography approach. Hum. Brain Mapp. 39, 1712–1720.

Andersson, J.L.R., Graham, M.S., Zsoldos, E., Sotiropoulos, S.N., 2016. Incorporating outlier detection and replacement into a non-parametric framework for movement and distortion correction of diffusion MR images. Neuroimage 141, 556–572.

Andersson, J.L., Skare, S., Ashburner, J., 2003. How to correct susceptibility distortions in spin-echo echo-planar images: Application to diffusion tensor imaging. Neuroimage 20, 870–888.

Andersson, J.L.R., Sotiropoulos, S.N., 2016. An integrated approach to correction for off-resonance effects and subject movement in diffusion MR imaging. Neuroimage 125, 1063–1078.

Balcer, L.J., 2006. Clinical practice. Optic neuritis. N Engl. J. Med. 354, 1273–1280.

Balcer, L.J., Galetta, S.L., Calabresi, P.A., Confavreux, C., Giovannoni, G., Havrdova, E., Hutchinson, M., Kappos, L., Lublin, F.D., Miller, D.H., O'Connor, P.W., Phillips, J.T., Polman, C.H., Radue, E.W., Rudick, R.A., Stuart, W.H., Wajgt, A., Weinstock-Guttman, B., Wynn, D.R., Lynn, F., Panzara, M.A., 2007. Natalizumab reduces visual loss in patients with relapsing multiple sclerosis. Neurology 68, 1299–1304.

Balcer, L.J., Raynowska, J., Nolan, R., Galetta, S.L., Kapoor, R., Benedict, R., Phillips, G., LaRocca, N., Hudson, L., Rudick, R., Multiple Sclerosis Outcome Assessments, C., 2017. Validity of low-contrast letter acuity as a visual performance outcome measure for multiple sclerosis. Mult. Scler 23, 734–747.

Balk, L.J., Steenwijk, M.D., Tewarie, P., Daams, M., Killestein, J., Wattjes, M.P., Vrenken, H., Barkhof, F., Polman, C.H., Uitdehaag, B.M., Petzold, A., 2015. Bidirectional trans-synaptic axonal degeneration in the visual pathway in multiple sclerosis. J. Neurol. Neurosurg. Psychiatry 86, 419–424.

Behrens, T.E., Berg, H.J., Jbabdi, S., Rushworth, M.F., Woolrich, M.W., 2007. Probabilistic diffusion tractography with multiple fibre orientations: What can we gain? Neuroimage 34, 144–155.

Chung, S., Fieremans, E., Wang, X., Kucukboyaci, N.E., Morton, C.J., Babb, J., Amorapanth, P., Foo, F.A., Novikov, D.S., Flanagan, S.R., Rath, J.F., Lui, Y.W., 2018. White matter tract integrity: An indicator of axonal pathology after mild traumatic brain injury. J. Neurotrauma 35, 1015–1020.

Compston, A., Coles, A., 2008. Multiple sclerosis. Lancet 372, 1502–1517.

Dale, A.M., Fischl, B., Sereno, M.I., 1999. Cortical surface-based analysis I. Segmentation and surface reconstruction. Neuroimage 9, 179–194.

de Kouchkovsky, I., Fieremans, E., Fleysher, L., Herbert, J., Grossman, R.I., Inglese, M., 2016. Quantification of normal-appearing white matter tract integrity in multiple sclerosis: A diffusion kurtosis imaging study. J. Neurol. 263, 1146–1155.

Desikan, R.S., Segonne, F., Fischl, B., Quinn, B.T., Dickerson, B.C., Blacker, D., Buckner, R.L., Dale, A.M., Maguire, R.P., Hyman, B.T., Albert, M.S., Killiany, R.J., 2006. An automated labeling system for subdividing the human cerebral cortex on MRI scans into gyral based regions of interest. Neuroimage 31, 968–980.

Fan, Q., Nummenmaa, A., Wichtmann, B., Witzel, T., Mekkaoui, C., Schneider, W., Wald, L., Huang, S., 2018. Validation of diffusion MRI estimates of compartment size and volume fraction in a biomimetic brain phantom using a human MRI scanner with 300 mT/m maximum gradient strength. Neuroimage 182, 469–478.

Fan, Q., Tian, Q., Ohringer, N., Nummenmaa, A., Witzel, T., Tobyne, S., Klawiter, E., Mekkaoui, C., Rosen, B., Wald, L., Salat, D., Huang, S., 2019. Age-related alterations in axonal microstructure in the corpus callosum measured by high-gradient diffusion MRI. Neuroimage 191, 325–336.

Fan, Q., Witzel, T., Nummenmaa, A., Van Dijk, K.R., Van Horn, J.D., Drews, M.K., Somerville, L.H., Sheridan, M.A., Santillana, R.M., Snyder, J., Hedden, T., Shaw, E.E., Hollinshead, M.O., Renvall, V., Zanzonico, R., Keil, B., Cauley, S., Polimeni, J.R., Tisdall, D., Buckner, R.L., Wedeen, V.J., Wald, L.L., Toga, A.W., Rosen, B.R., 2016. MGH-USC Human Connectome Project datasets with ultra-high b-value diffusion MRI. Neuroimage 124, 1108–1114.

Fieremans, E., Jensen, J.H., Helpern, J.A., 2011. White matter characterization with diffusional kurtosis imaging. Neuroimage 58, 177–188.

Fieremans, E., Benitez, A., Jensen, J.H., Falangola, M.F., Tabesh, A., Deardorff, R.L., Spampinato, M.V., Babb, J.S., Novikov, D.S., Ferris, S.H., Helpern, J.A., 2013. Novel white matter tract integrity metrics sensitive to Alzheimer disease progression. AJNR Am. J. Neuroradiol. 34, 2105–2112.

Fischl, B., Rajendran, N., Busa, E., Augustinack, J., Hinds, O., Yeo, B.T., Mohlberg, H., Amunts, K., Zilles, K., 2008. Cortical folding patterns and predicting cytoarchitecture. Cereb. Cortex 18, 1973–1980.

Gabilondo, I., Martinez-Lapiscina, E.H., Martinez-Heras, E., Fraga-Pumar, E., Llufriu, S., Ortiz, S., Bullich, S., Sepulveda, M., Falcon, C., Berenguer, J., Saiz, A., Sanchez-Dalmau, B., Villoslada, P., 2014. Trans-synaptic axonal degeneration in the visual pathway in multiple sclerosis. Ann. Neurol. 75, 98–107.

Greve, D.N., Fischl, B., 2009. Accurate and robust brain image alignment using boundary-based registration. Neuroimage 48, 63–72.

Horbruegger, M., Loewe, K., Kaufmann, J., Wagner, M., Schippling, S., Pawlitzki, M., Schoenfeld, M.A., 2019. Anatomically constrained tractography facilitates biologically plausible fiber reconstruction of the optic radiation in multiple sclerosis. Neuroimage Clin. 22, 101740.

Huang, S., Fan, Q., Machado, N., Eloyan, A., Bireley, J., Russo, A., Tobyne, S., Patel, K., Brewer, K., Rapaport, S., Nummenmaa, A., Witzel, T., Sherman, J., Wald, L., Klawiter, E., 2019. Corpus callosum axon diameter relates to cognitive impairment in multiple sclerosis. Ann Clin Transl Neurol 6, 882–892.

Huang, S., Nummenmaa, A., Witzel, T., Duval, T., Cohen-Adad, J., Wald, L., McNab, J., 2015. The impact of gradient strength on in vivo diffusion MRI estimates of axon

diameter. Neuroimage 106, 464–472.
Huang, S., Tian, Q., Fan, Q., Witzel, T., Wichtmann, B., McNab, J., Bireley, J., Machado, N., Klawiter, E., Mekkaoui, C., Wald, L., Nummenmaa, A., 2020. High-gradient diffusion MRI reveals distinct estimates of axon diameter index within different white matter tracts in the in vivo human brain. Brain Structure and Function 225, 1277–1291.
Huang, S., Tobyne, S., Nummenmaa, A., Witzel, T., Wald, L., McNab, J., Klawiter, E., 2016. Characterization of Axonal Disease in Patients with Multiple Sclerosis Using High-Gradient-Diffusion MR Imaging. Radiology 280, 244–251.
Iglesias, J.E., Insausti, R., Lerma-Usabiaga, G., Bocchetta, M., Van Leemput, K., Greve, D.N., van der Kouwe, A., Alzheimer's Disease Neuroimaging I, Fischl, B., Caballero-Gaudes, C., Paz-Alonso, P.M., 2018. A probabilistic atlas of the human thalamic nuclei combining ex vivo MRI and histology. Neuroimage 183, 314–326.
Jensen, J.H., Helpern, J.A., Ramani, A., Lu, H., Kaczynski, K., 2005. Diffusional kurtosis imaging: the quantification of non-gaussian water diffusion by means of magnetic resonance imaging. Magn. Reson. Med. 53, 1432–1440.
Jensen, J.H., Helpern, J.A., 2010. MRI quantification of non-Gaussian water diffusion by kurtosis analysis. NMR Biomed. 23, 698–710.
Keil, B., Blau, J.N., Biber, S., Hoecht, P., Tountcheva, V., Setsompop, K., Triantafyllou, C., Wald, L.L., 2013. A 64-channel 3T array coil for accelerated brain MRI. Magn. Reson. Med. 70, 248–258.
Klawiter, E.C., Schmidt, R.E., Trinkaus, K., Liang, H.F., Budde, M.D., Naismith, R.T., Song, S.K., Cross, A.H., Benzinger, T.L., 2011. Radial diffusivity predicts demyelination in ex vivo multiple sclerosis spinal cords. Neuroimage 55, 1454–1460.
Klistorner, A., Sriram, P., Vootakuru, N., Wang, C., Barnett, M.H., Garrick, R., Parratt, J., Levin, N., Raz, N., Van der Walt, A., Masters, L., Graham, S.L., Yiannikas, C., 2014. Axonal loss of retinal neurons in multiple sclerosis associated with optic radiation lesions. Neurology 82, 2165–2172.
Klistorner, A., Vootakuru, N., Wang, C., Yiannikas, C., Graham, S.L., Parratt, J., Garrick, R., Levin, N., Masters, L., Lagopoulos, J., Barnett, M.H., 2015. Decoding diffusivity in multiple sclerosis: Analysis of optic radiation lesional and non-lesional white matter. PLoS One 10, e0122114.
Lindemer, E.R., Salat, D.H., Smith, E.E., Nguyen, K., Fischl, B., Greve, D.N., Alzheimer's Disease Neuroimaging I, 2015. White matter signal abnormality quality differentiates mild cognitive impairment that converts to Alzheimer's disease from nonconverters. Neurobiol. Aging 36, 2447–2457.
London, F., Zephir, H., Drumez, E., Labreuche, J., Hadhoum, N., Lannoy, J., Hodel, J., Vermersch, P., Pruvo, J.P., Leclerc, X., Outteryck, O., 2019. Optical coherence tomography: A window to the optic nerve in clinically isolated syndrome. Brain 142, 903–915.
Margoni, M., Petracca, M., Schiavi, S., Fabian, M., Miller, A., Lublin, F.D., Inglese, M., 2019. Axonal water fraction as marker of white matter injury in primary-progressive multiple sclerosis: A longitudinal study. Eur. J. Neurol. 26, 1068–1074.
McNab, J., Edlow, B., Witzel, T., Huang, S., Bhat, H., Heberlein, K., et al., 2013. The Human Connectome Project and beyond: initial applications of 300 mT/m gradients. Neuroimage 80, 234–245.
Oberwahrenbrock, T., Schippling, S., Ringelstein, M., Kaufhold, F., Zimmermann, H., Keser, N., Young, K.L., Harmel, J., Hartung, H.P., Martin, R., Paul, F., Aktas, O., Brandt, A.U., 2012. Retinal damage in multiple sclerosis disease subtypes measured by high-resolution optical coherence tomography. Mult. Scler. Int. 2012, 530305.
Raz, N., Bick, A.S., Ben-Hur, T., Levin, N., 2015. Focal demyelinative damage and neighboring white matter integrity: An optic neuritis study. Mult. Scler. 21, 562–571.
Reich, D.S., Smith, S.A., Gordon-Lipkin, E.M., Ozturk, A., Caffo, B.S., Balcer, L.J., Calabresi, P.A., 2009. Damage to the optic radiation in multiple sclerosis is associated with retinal injury and visual disability. Arch. Neurol. 66, 998–1006.
Rocca, M.A., Mesaros, S., Preziosa, P., Pagani, E., Stosic-Opincal, T., Dujmovic-Basuroski, I., Drulovic, J., Filippi, M., 2013. Wallerian and trans-synaptic degeneration contribute to optic radiation damage in multiple sclerosis: a diffusion tensor MRI study. Mult. Scler. 19, 1610–1617.
Schmierer, K., Wheeler-Kingshott, C.A., Boulby, P.A., Scaravilli, F., Altmann, D.R., Barker, G.J., Tofts, P.S., Miller, D.H., 2007. Diffusion tensor imaging of post mortem multiple sclerosis brain. Neuroimage 35, 467–477.
Sepulcre, J., Murie-Fernandez, M., Salinas-Alaman, A., Garcia-Layana, A., Bejarano, B., Villoslada, P., 2007. Diagnostic accuracy of retinal abnormalities in predicting disease activity in MS. Neurology 68, 1488–1494.
Setsompop, K., Kimmlingen, R., Eberlein, E., Witzel, T., Cohen-Adad, J., McNab, J., et al., 2013. Pushing the limits of in vivo diffusion MRI for the Human Connectome Project. Neuroimage 80, 220–233.
Smith, S.M., Jenkinson, M., Woolrich, M.W., Beckmann, C.F., Behrens, T.E., Johansen-Berg, H., Bannister, P.R., De Luca, M., Drobnjak, I., Flitney, D.E., Niazy, R.K., Saunders, J., Vickers, J., Zhang, Y., De Stefano, N., Brady, J.M., Matthews, P.M., 2004. Advances in functional and structural MR image analysis and implementation as FSL. Neuroimage 23 (Suppl 1), S208–S219.
Tian, Q., Wintermark, M., Jeffrey Elias, W., Ghanouni, P., Halpern, C.H., Henderson, J.M., Huss, D.S., Goubran, M., Thaler, C., Airan, R., Zeineh, M., Pauly, K.B., McNab, J.A., 2018. Diffusion MRI tractography for improved transcranial MRI-guided focused ultrasound thalamotomy targeting for essential tremor. Neuroimage Clin. 19, 572–580.
Toledo, J., Sepulcre, J., Salinas-Alaman, A., Garcia-Layana, A., Murie-Fernandez, M., Bejarano, B., Villoslada, P., 2008. Retinal nerve fiber layer atrophy is associated with physical and cognitive disability in multiple sclerosis. Mult. Scler 14, 906–912.
Tur, C., Goodkin, O., Altmann, D.R., Jenkins, T.M., Miszkiel, K., Mirigliani, A., Fini, C., Gandini Wheeler-Kingshott, C.A., Thompson, A.J., Ciccarelli, O., Toosy, A.T., 2016. Longitudinal evidence for anterograde trans-synaptic degeneration after optic neuritis. Brain 139, 816–828.
Veraart, J., Sijbers, J., Sunaert, S., Leemans, A., Jeurissen, B., 2013. Weighted linear least squares estimation of diffusion MRI parameters: Strengths, limitations, and pitfalls. Neuroimage 81, 335–346.
Yu, F., Fan, Q., Tian, Q., Ngamsombat, C., Machado, N., Bireley, J., Russo, A., Nummenmaa, A., Witzel, T., Wald, L., Klawiter, E., Huang, S., 2019. Imaging G-Ratio in Multiple Sclerosis Using High-Gradient Diffusion MRI and Macromolecular Tissue Volume. Am J Neuroradiol 40, 1871–1877.
Zimmermann, H., Freing, A., Kaufhold, F., Gaede, G., Bohn, E., Bock, M., Oberwahrenbrock, T., Young, K.L., Dorr, J., Wuerfel, J.T., Schippling, S., Paul, F., Brandt, A.U., 2013. Optic neuritis interferes with optical coherence tomography and magnetic resonance imaging correlations. Mult. Scler 19, 443–450.